Radiation Physics and Chemistry 166 (2020) 108512

Contents lists available at ScienceDirect

Radiation Physics and Chemistry

journal homepage: www.elsevier.com/locate/radphyschem

The effects of 5 MeV carbon ion irradiation on micro-fine grain graphite

Muhammad Zubair[a,b,c,*], Rafik Hazem[e], Ishaq Ahmad[b,f], M. Imtiaz Khan[d], Ting-kai Zhao[f,g], Hazrat Ali[d], Tariq Ali[j], Muhammad Arshad[b,f], Fida Rehman[d], Pervaiz Ahmad[i], Mahmoud Izerrouken[h]

[a] College of Materials Science and Engineering, Key Laboratory of Advanced Functional Materials, Ministry of Education, Beijing, University of Technology, Beijing, 100124, China
[b] National Center for Physics, Islamabad, 44000, Pakistan
[c] Center of Excellence in Solid State Physics, University of the Punjab, Lahore, Pakistan
[d] Department of Physics, Abbottabad University of Science and Technology, Havelian, Khyber Pakhtunkhwa, Pakistan
[e] URMPE Unit, University M'Hamed Bougara Boumerdes, 35000, Boumerdes, Algeria
[f] NPU-NCP Joint International Research Center on Advanced Nanomaterials and Defects Engineering, Northwestern Polytechnical University, Xi'an, 710072, China
[g] School of Materials Science & Engineering, Northwestern Polytechnical University, Xi'an, 710072, China
[h] Nuclear Research Centers of Draria, BP. 43, Algiers, Algeria
[i] Department of Physics, University of Azad Jammu and Kashmir, 13100, Muzaffarabad, Pakistan
[j] Department of Physics, United Arab Emirates University, Al Ain, United Arab Emirates

ARTICLE INFO

Keywords:
Ions irradiation
Graphite
Structural damage
Irradiation temperature
Graphitization
Disorder

ABSTRACT

5 MeV carbon ion irradiation effects on micro-fine grain graphite samples are investigated. The X-ray diffraction (XRD), Raman spectroscopy, field emission scanning electron microscope (FESEM), and high-resolution transmission electron microscope (HRTEM) are used to study changes due to irradiation. At a dose of 0.5 dpa, the isolated defects (monovacancies) were generated with a low density within graphitic regions, which contribute considerably to the sharp reduction of graphitic amount in irradiated material but insignificantly to the activation of Raman disordered band. HRTEM images show the accumulation of these defects in clusters between (002) basal planes leading to the increase of lattice parameter and d-spacing in c-direction. Samples irradiated with a dose of 1 dpa initiate an annealing process in the material resulting in defects annihilation. The enhancement of the graphitization degree is obviously correlated with the reduction of disordered material. After irradiation of high dose (3–5 dpa), **the high concentration of defects leads to the formation of stable planar V_6 rings.** These rings are found to survive even at the higher temperature, but the graphitization degree remains nearly unchanged.

1. Introduction

The molten salt reactor (MSR) is one of the six Generation-IV reactors (Abram, 2002) that uses a fluid fuel in the form of very hot molten fluoride or chloride salt instead of the solid fuel used in most reactors. Graphite is mostly used as a neutron moderator to control the flow patterns of the fuel salt in the MSR (Rosenthal et al., 1972). **Most irradiated graphite is related to the reactor moderators and reflectors as well, but there are some other routes from which radioactive graphite component needs absolute disposal, for example, contaminated graphite tools, graphite crucibles and moulds for the production of nuclear fuel assemblies** (Tian et al., 2010)**.** The micro-fine grain graphite ZXF-5Q (grain size $< 1\,\mu m$) is a promising candidate for the MSR (Zhang et al., 2016). It has been reported that only micro-fine grain graphite ZXF-5Q has the entrance pore diameters below 2 μm and it could consequently prevent the molten salt impregnation in the relative high-pressure environment. Hence, graphite materials have very good irradiation and impregnation behaviour (Zhang et al., 2016) which is highly dependable on their microstructures (FengXu. et al., 2013).

The interaction of neutrons with the graphite matrix via elastic collision involves the displacement of the carbon atoms that are ejected from their original site. These recoil atoms, if they are sufficiently energetic, will in turn be able to eject other atoms and create displacement cascades resulting in electronic excitation and ionization (Sahaet al., 2018). Hence, ion beam irradiation can be used to replace the neutron irradiation to simulate damage in materials. It was used effectively to investigate structural damages and to generate defects in graphite that

* Corresponding author. National Center for Physics, Islamabad 44000, Pakistan.
E-mail address: zubairphy@emails.bjut.edu.cn (M. Zubair).

https://doi.org/10.1016/j.radphyschem.2019.108512
Received 14 May 2019; Received in revised form 1 October 2019; Accepted 3 October 2019
Available online 09 October 2019
0969-806X/

could be like those induced by neutrons in nuclear reactors (Irradiation damage in gra, 2000). Furthermore, the ion irradiation has many advantages, for example, the higher doses can be achieved comparatively to the neutron irradiation and these doses allow to achieve higher amounts of displacements per atom (dpa) in short times.

In general, there are two mechanisms used to describe the travelling of energetic ions in matter. One is called as the nuclear energy loss and second is known as the electronic energy loss. The former is accredited to the low ion energy regime (< 100 KeV/u) where the change in energetic ions is occurred because of the elastic collision and the latter case refers to the higher energy regime (> 1 MeV/u) where the excitation and ionization of an atom happens due to the inelastic collision. In the medium range of energy, the electronic energy loss is the leading process comparatively to the nuclear energy loss (Sigmund, 2004; Ziegler et al., 2010; Spohr, 1990).

In this work, we use high energy ions to attain structural changes in materials (Zhou et al., 2017**). At the low energy regime, the target atom vacancies could be generated and then displaced to the interstitial sites. These large defects could possibly modify the basic properties of materials used** (Ziegler et al., 2010)**.** Furthermore, we can also avoid a problem of radioactivity because there is no sample activation. The study of irradiation effects on graphite paves the way to better understanding of the ion-matter interactions in other carbon allotropes.

Knowing that the carbon atoms are the recoil particles in neutron irradiated graphite, the study of the induced damage caused by their interaction is of great interest. In this article, 5 MeV C^{++} ion beam irradiation effects on the structural properties of micro-fine grain graphite ZXF-5Q were studied using X-ray diffraction, Raman spectroscopy, field emission scanning electron microscopy and high-resolution transmission electron microscopy techniques. The nature of irradiation-induced defects in graphite is investigated as well.

2. Experimental details

In this work, graphite ZXF-5Q purchased from POCO Graphite Inc was used for irradiation study. The experiment was performed to investigate the effects of Carbon (C^{++}) ions irradiation on the structural properties of micro-fine grain graphite samples with the help of 5 MeV-Pelletron Tandem accelerator (model number 5UDH USA) at room temperature under pressure of $\sim 10^{-7}$ Torr at the National Centre for Physics, Islamabad, Pakistan. **Uniform irradiation was achieved by using a beam scanner combined with a set of four independent slits, which were mounted between the quadrupole magnet and the sample position.**

Five samples were irradiated with various doses of carbon (C^{++}) ions, 0.15 dpa **(1 dpa = 5 × 10^{15} ions/cm^2),** 0.5 dpa, 1 dpa, 3 dpa, 5 dpa, while one was kept un-irradiated as a reference. These five samples, which will be exposed to carbon ions, were mounted on a metal strip with the aid of polymeric fixer. This strip was mounted on a target holder of the accelerator. The diameter of the beam was 8 mm × 8 mm which irradiated the sample surface uniformly, so the carbon ions remained uniform over the whole surface. Each sample was irradiated at the same energy 5 MeV and current 100 nA. **All samples were irradiated without additional current heating and were only heated by the ion beam irradiation achieving average temperature up to 300°C due to the large ion beam flux.** The irradiated samples were investigated by several methods. XRD (Model Bruker D8 Co. Ltd loaded with Cu Kα radiation **(λ = 15.40598 Å)** scan rate 2°, voltage 40 kV, tube current 35 mA, 2θ range 20°–60°, was used to characterize the structural analysis of all un-irradiated and irradiated samples. Raman spectroscopy (Model Lab Ram III DongWoo OPTRON South Korea) measurements were performed at room temperature using a 150 mW Ar^{+} laser beam of a wavelength of 514.8 nm in frequency range 1000–2000 cm^{-1}. The microstructures of samples were characterized by HRTEM (JEM 3010 (JEOL)) and the surface morphology was examined by FESEM (Model MIRA-3 TESCAN).

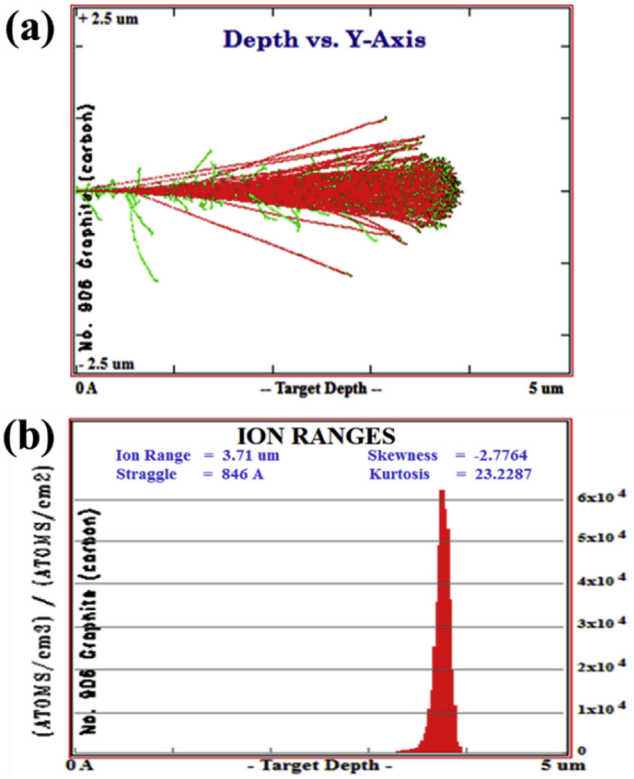

Fig. 1. SRIM visual representation of the 5 MeV C^{++} (a) ion distribution depth where green represents displaced carbon atoms and red represents the ion path and (b) ion ranges in the target graphite, respectively. (For interpretation of the references to colour in this figure legend, the reader is referred to the Web version of this article.)

The heavy carbon ion beam causes deformation of the material in the graphite layered lattice. The lattice variation is mainly caused by the electronic stopping and the interaction of the incident ions with the nucleus of the target atom. Ionization is an important factor under such high beam energies, whereas nuclear interactions prevail in the projected range. Using the stopping/range of ions in matter (SRIM, 2008) we found the penetration depth of carbon ions in graphite up to 3.71 μm and the vacancies generated per ions are around 533.2. This is the allowable range of carbon ion beams with 5 MeV. Skewness is found −2.77 and kurtosis 23.33. Fig. 1a and b shows calculated SRIM visual representation of the 5 MeV C^{++} ion distribution depth and ion range in the target graphite.

3. Results and discussion

3.1. X ray diffraction

The XRD patterns of un-irradiated and irradiated samples are depicted in Fig. 2a. The Miller indices (h, k, l) were matched with the ICDD-PDF #-041-1487 which demonstrated that the samples have hexagonal structures, with P63/mmc space group. The samples are polycrystalline in nature, fact evidenced by the presence of four peaks located respectively at 26.67°, 42.73°, 44.5° and 54.5° corresponding to (002), (100), (101) and (004) planes, where (002) is the strongest. This significant peak provides important information about the structural changes of the material which are identified through its shape analysis. It can also be seen that the original crystalline structure was maintained after ions irradiation, manifested by the presence of all pre-existing peaks and the absence of new ones (see Fig. 2).

In order to follow the evolution of peaks with ions irradiation, the

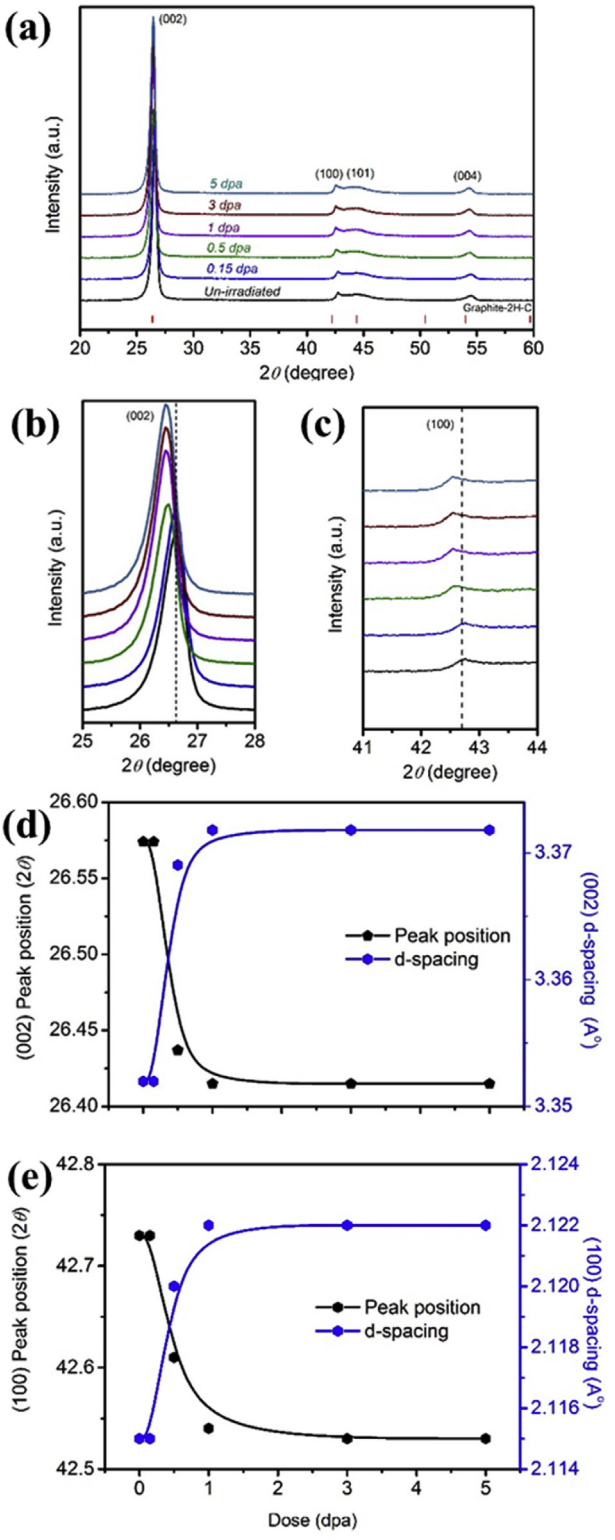

Fig. 2. (a) XRD standard pattern of phase and patterns of un-irradiated and irradiated micro-fine grain graphite ZXF-5Q sample; The enlarged view in the 2θ range peak shifting of (b) 25°–28°, and (c) 41°–44°, and its corresponding d-spacing vs. Dose (dpa) of (d) (002) and (e) (100) direction.

(002) peak due to c-direction and (100) peak corresponding to a-direction in the lattice, are separately presented in the enlarged view angles 25°–28° and 41°–44° range in Fig. 2b and c respectively. In these figures it is clearly seen that the peak due to c-axis is expanded but the peak due to a-axis is shrunk. These effects are happened due to the expansion between the graphite layers that triggered by the bombardment-induced defects, i.e. defect accumulation between the basal planes. In fact, ion irradiation displaces atoms from the graphitic planes, causing crystal expansion in the c-axis and shrinking in the a-axis.

On the other hand, the evolution of (002) and (100) peak position and their corresponding interlayer d-spacing (distance between consecutive basal layers) as function of ions dose, are respectively reported in Fig. 2d and e. The value of interlayer spacing d_{002} (in c-direction) and d_{001} (in a-direction) was calculated from Bragg equation **($n\lambda = 2d\sin\theta$)** where λ is the wavelength of X-rays in Å and θ is the scattering angle in radians. It is worth noting firstly that d-spacing values varies accordance with a literature (Galy et al., 2017; Ammar et al., 2015). Furthermore, the calculated d002 value of the irradiated sample (~0.373 nm) is larger than that of a typical graphite structure (~0.338 nm), but it is similar to that of the disordered form, which is well known as "turbostratic graphite" (Li et al., 2007; Binder et al., 2017).

The increase in (002) d-spacing is very obvious, from 3.35 Å to 3.38 Å, which helps to justify the expansion along the c-axis. In addition, it should be noted that the d-spacing in the c-direction is very large compared to the a-direction, and the relative change is significant (Pellemoine et al., 2015)**.** Hence, the increase of d-spacing in irradiated samples may be induced by defects accumulation between basal layers. Furthermore, it has been observed that when ion beam penetrates inside material gathers and forms some clusters colonies between plans leading to the increase of d-spacing (Pellemoine et al., 2015; Sigmund, 2004). Thus, we deduce that the irradiation effect is developed mainly along c-direction where the stress induced by carbon ions is more intense.

3.2. Raman spectroscopy

In order to better understand the material behaviour under carbon ion irradiation, Raman spectroscopy was performed on un-irradiated and irradiated samples. Fig. 3a shows the Raman spectra of the un-irradiated sample in comparison to irradiated sample at different irradiation doses. Two peaks located at 1601 cm^{-1} and 1370 cm^{-1} are observed in Raman spectra of all samples and attributed respectively to G and D bands in micro-fine grain graphite. In graphite, the G band is the most prominent feature and is considered as the finger print peak of material (Kwiecinska et al., 2010; Nemanich and Solin, 1979). This peak, corresponding to the first order Raman scattering, is due to double degenerate phonon mode E_{2g} of basal plane vibrations (Dresselhaus et al., 2010; Ni et al., 2010), that characterizes the relative motion between 2 sp^2 carbon atoms (Ferrari, 2007). The second most important peak D, originating from A_{1g} ring breathing mode (Tan et al., 2013), is the feature of the double-resonance Raman scattering (Maultzsch et al., 2004). The D peak reflects the disorder in the material and thus is symmetrically forbidden in perfect graphite. Compared to the G peak, it has a dispersive nature and its position can be moved with the change of excitation energy (Maultzsch et al., 2004). D mode is always present in natural polycrystalline graphite, but it will be Raman inactive in single crystal because it is forbidden by the k conservation rules (Tan et al., 2013). Raman spectrum of the un-irradiated sample in Fig. 3a shows that the disordered peak D is wider than the graphitic peak G. This result indicates the high degree of graphitization and low disorder of un-irradiated sample. Moreover, the Raman bands' intensity of irradiated samples is clearly higher than that of the un-irradiated one, while their position remains unchanged.

In order to assess the degree of graphitization and evaluate the discrimination of the defect types in irradiated samples, one can use the combination of the quantified intensity ratio I_D/I_G and full width at half maximum (FHWM) of G peak. These two indicators of structural disorder vary differently as both depend on the nature and concentration of the generated defects. Indeed, I_D/I_G ratio reflects the disorder in the

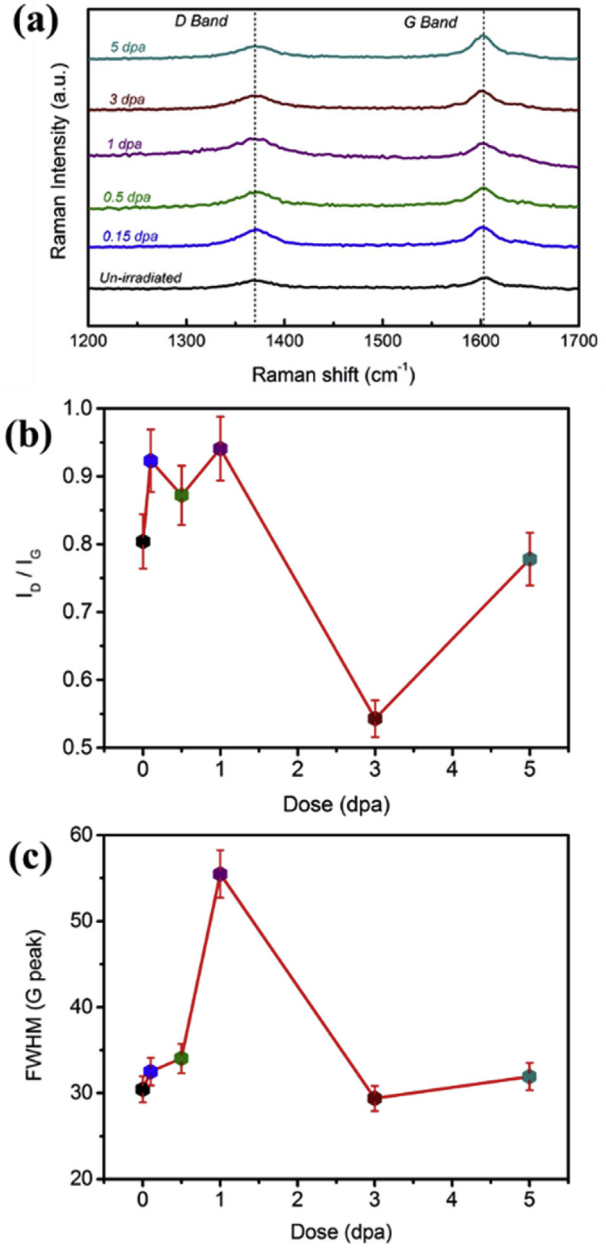

Fig. 3. (a) Raman spectra of the un-irradiated and irradiated micro-fine grain graphite ZXF-5Q sample; (b) Intensity ratio I_D/I_G vs. Dose (dpa) and (c) variation of FWHM of the Raman G peak vs. Dose (dpa). **The error bars reflect the experimental variance andanalytical error.**

lattice, which comes from different types of defects (point defects or dislocations). On the other hand, the FWHM of G peak reveals the graphitization degree of materials (Ammar et al., 2015). Hence, I_D/I_G ratio and FWHM of G peak versus irradiation doses were plotted in Fig. 3b and c respectively. In the first dose range ($\leq$1 dpa), it is observed that the I_D/I_G ratio increases with increasing dose. This response could be due to irradiation created defects in the material. Meanwhile, the FWHM of G peak increases slightly up to the dose of 0.5 dpa and further shows a drastic increase up to 1 dpa. This behaviour reflects the strong reduction of graphitization degree in irradiated sample. These observations indicate the non-correlation between the I_D/I_G ratio and FWHM of G band which means that the generated defects contribute insignificantly to the activation of the disordered band D. Therefore, the behaviour of this material can be explained by the ion irradiation creating isolated defects with low density (monovacancies) within graphitic regions, which leads to the local disorder. The increase of the structural disorder is also reported by Deslandes et al. (2014) in 5 MeV C^{++} irradiated graphite with nearly the same dose range. Further increase in dose up to 3 dpa decrease drastically the I_D/I_G ratio and FWHM of G-band. This behaviour reflects the enhancement of graphitic amount in the sample which is correlated with the reduction of disordered material. This enhancement can be attributed to the reduction of defects concentration inside the material. This behaviour was firstly explained by the mutual annihilation of in-plane defects with mobile interstitials (Niwase and Tanabe, 1993). **With increasing irradiation dose, the electron excitation causes lattice vibrations which results in heating of the sample. As reported previously in Refs** (Mitchel and Taylor, 1965; Shi et al., 2016; Latham et al., 2013) **that an increase in environment temperature rises an annealing process in a sample due to which the Wigner energy is released. The expected release of Wigner energy may be very small to restore complete damage and actual crystallinity of the material, although due to in-plane defects and mutual annihilation of the mobile interstitials, improve the graphitization of materials to some extent at 3 dpa. The tendency of the layer spacing to decrease is related to the complete recovery of the radiation damage annealed at very high temperatures of $\geq$ 1500 °C, where the layer spacing d(002) of graphite decreases with increasing crystallinity. In fact, recombination of interstitials and vacancies may occur due to the high ion beam excitation. When the temperature goes above 140 K, the role of vacancies in annealing process begins and the intimate Frenkel defects starts annihilating as well. Even at room temperature, the annealing process along with annihilation of intimate Frenkel defects continues. Further by increasing the temperature up to 475 K, the vacancies turn out to be completely mobile to annihilate adjacent interstitials and the Wigner energy is released.**

Furthermore, Krishna et al. (2017) have reported the effects of temperature during irradiation. This annealing process results in the recombination of interstitial atoms and vacancies (Krishna et al., 2017). The competition between defects generation and their annihilation during irradiation has also been reported in neutron irradiation induced damage in graphite (Telling and Heggie, 2007). In other words, the isolated defects (monovacancies) generated during the dose and other pre-existing ones, will be annihilated at some sinks in material. Indeed, the annihilation process becomes predominant over the defects production and enhances the graphitization process inside the material.

When the annihilation process becomes dominant and it leads to an increase in the degree of graphitization within the material. At high doses, high concentrations of defects result in the formation of a stable planar V6 ring, but the degree of graphitization remains almost unchanged. When the dose exceeds 3 dpa, the sudden change in the $\boldsymbol{I_D/I_G}$ ratio shows a sharp increase, while the FWHM (G) remains almost unchanged (Fig. 3b and c). The increase in the $\boldsymbol{I_D/I_G}$ ratio is a sign of the disordered material enhancement after the defect is generated. Therefore, in the samples irradiated with 5 dpa, the defect concentration was high, and they participated in the activation of the disordered band D without changing the local structural order. This result means that the two samples irradiated with 3 and 5 dpa are also graphitized, but are not equally filled by defects.

Similar phenomena were also observed earlier in ion irradiated nuclear graphite (Ammar et al., 2015). By comparing the material response between both dose ranges (0–1 dpa) and (3–5 dpa), in which the defects production was the predominant process, it can be deduced that the nature of the created defects (clusters) are obviously different. Furthermore, it can even be predicted that the defects created at higher doses should be relatively stable and remain even at high temperatures. Moreover, it has been reported that the irradiation temperature raises the threshold energy for atomic displacement (E_d) as the interstitial-vacancy separation distance, required to produce a stable Frenkel-pair, is increased (Krishna et al., 2017). **In this context,** Tang et al. (1999)

suggest an aggregation structure formed by 6 vacancies (V_6) as the possible stable clusters generated by irradiation in graphite. In fact, with increasing temperature, resulting from increasing dose, monovacancies of high densities are created through collisional cascades. These monovacancies will get enough energy to move through the lattice and develop clusters of vacancies leading to the formation of planar V_6 rings (Telling and Heggie; Sigmund, 2004)**.**

Considering the first principle calculation and the positron annihilation process, the planar V_6 ring is an aggregate of six vacancies forming a closed six ring and has been considered to have high stability in irradiated graphite. Calculations show that vacancy clusters are the most likely defect structures because they are energetically favourable and stable, which is believed to survive the 1700 K anneal (Telling and Heggie, 2007; Tang et al., 1999; Li. et al., 2019)**. C. Q. Shi et al. also found that high-dose irradiation vacancy complexes (stable V_6 rings) were established and stabilized at temperatures around 1400 K** (Shi et al., 2016)**.** In the light of above reports, based on the combination of the I_D/I_G and FWHM (G), the discrimination of the defect types was demonstrated.

3.3. Field emission scanning electron microscopy (FESEM)

FESEM images of un-irradiated and those irradiated at 1 dpa, 3 dpa and 5 dpa micro-fine grain graphite ZXF-5Q samples are shown in Fig. 4a–d. The morphology before irradiation was fine, smooth and regular shape microstructure, but completely converted to nano-crowded sheets after carbon ion beam treatment, which showed damage and formation of defective nanoclusters. Heavy carbon ion beam irradiation produces hot spikes inside and outside the surface of the material. The heat spikes generate annealing temperature which suffer the material surface morphology. This temperature may have the milling effect which is believed to be the result of a smooth surface transition to nanosheets, nanostructures. (Production of atomic disp, 1956; Mironov et al., 2015).

3.4. High resolution transmission electron microscope (HRTEM)

A combined study of HRTEM and Raman spectroscopy of carbon

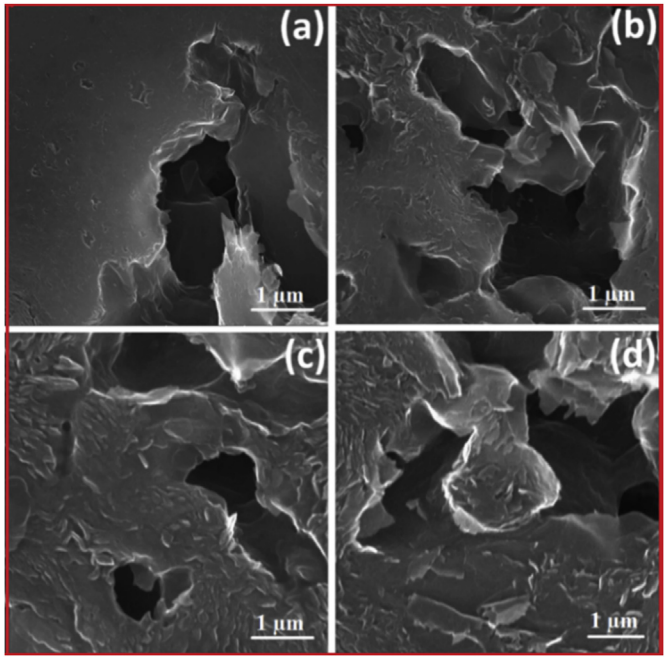

Fig. 4. (a–d) SEM images of un-irradiated and irradiated micro-fine grain graphite ZXF-5Q sample: (a) un-irradiated, (b) 1 dpa, (c) 3 dpa, (d) 5 dpa.

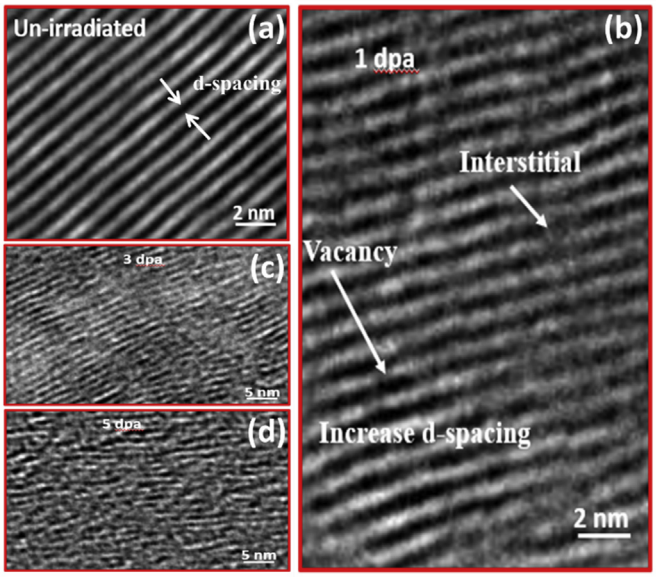

Fig. 5. (a–d) HRTEM images of un-irradiated and irradiated micro-fine grain graphite ZXF-5Q sample: (a) un-irradiated, (b) 1 dpa, (c) 3 dpa, (d) 5 dpa.

irradiated graphite can provide more information on the irradiation produced damage in POCO grade ZXF-5Q graphite. The HRTEM images of the un-irradiated sample and those irradiated at 1, 3 and 5 dpa are given in Fig. 5a–d. The un-irradiated sample demonstrates a flawless spatial arrangement of graphite layers with a constant interlayer spacing d_{002} around 0.35 nm. Moreover, the sample irradiated at 1 dpa displays a structural degradation illustrated by tortuosity (or curvature) of the (002) planes, accompanied by an increase of interlayer spacing d_{002}, previously reported in XRD spectra (Fig. 2d). Hence, the changes produced in the irradiated sample could be due to the accumulations of point defects (clusters), as observed in Fig. 5b, which would have disordered the lattice. This disorder was also evidenced by the increase of I_D/I_G ratio in this range dose (Fig. 3b). These HRTEM observations suggest the breakup of the graphitic structure into nanocrystalline regions with increasing dose (Gotoh. et al., 1989), also corroborated by Raman analysis revealing the reduction of graphitization degree in this range dose. Furthermore, comparing the HRTEM images of the samples irradiated with 3 dpa and 5 dpa, turbulence and disordering of the basal plane are clearly manifested in the lattice image of the sample irradiated with 5 dpa. The turbulence and disordering in the lattice should originate from irregularity of the bonding angle and length (Niwase and Tanabe, 1993), which causes the broadening of the Raman spectra as indicated in Fig. 3c. These results are aligned with those obtained by Raman analysis in the previous section where the I_D/I_G ratio increase in this dose range (Fig. 3b).

4. Conclusions

The damage induced in POCO grade ZXF-5Q graphite irradiated with 5 MeV C^{++} was investigated by XRD, Raman spectroscopy, FESEM, and HRTEM. The isolated defects with a low density are generated within graphitic regions at low doses and thus contribute insignificantly to the activation of Raman disordered band. In addition, a sharp reduction of graphitization degree occurs in the irradiated material. It has been observed via HRTEM that the created defects accumulate in clusters between basal planes and lead to the increase of lattice parameter and d-spacing mainly in c-direction. With further increasing dose, the irradiation temperature increases and initiates an annealing process in the material resulting in defects annihilation, which was already competing with damage production. The annihilation process becomes predominant and leads to the enhancement of the

graphitization degree within material. At high doses, the high concentration of defects leads to the formation of stable planar V_6 rings, which survives even at higher temperature, but the graphitization degree remains nearly unchanged. Hence, the samples are equally graphitized, but not equally populated by defects.

Declaration of competing interest

The authors declare that they have no known competing financial interests or personal relationships that could have appeared to influence the work reported in this paper.

Acknowledgments

The iThemba LABS, UNESCO, HEC and TWAS are gratefully acknowledged.

Appendix A. Supplementary data

Supplementary data to this article can be found online at https://doi.org/10.1016/j.radphyschem.2019.108512.

References

Abram, Timothy, 2002. A Technology Roadmap for Generation-IV Nuclear Energy Systems, USDOE/GIF-002-00. United States Department of Energy A Technology Roadmap for Generation-IV Nuclear Energy Systems, USDOE/GIF-002-00.
Ammar, M.R., Galy, N., Rouzaud, J.N., Toulhoat, N., Vaudey, C.E., Simon, P., Moncoffre, N., 2015. Characterizing various types of defects in nuclear graphite using Raman scattering: heat treatment, ion irradiation and polishing. Carbon 95, 364–373.
Binder, C., Bendo, T., Hammes, G., Neves, G.O., Binder, R., de Mello, J.D.B., Klein, A.N., 2017. Structure and properties of in situ-generated two-dimensional turbostratic graphite nodules. Carbon 124, 685–692.
Deslandes, Alec, Guenette, Mathew C., Corr, CormacS., Karatchevtseva, Inna, Thomsen, Lars, Ionescu, Mihail, Lumpkin, GregoryR., Riley, DanielP., 2014. Ion irradiated graphite exposed to fusion-relevant deuterium plasma. Nucl. Instr. Meth. Phys. 340, 21–26.
Dresselhaus, M.S., Jorio, A., Souza Filho, A.G., Saito, R., 2010. Defect characterization in graphene and carbon nanotubes using Raman spectroscopy. Philos. Trans. A. Math. Phys. Eng. Sci. 368, 5355–5377.
Feng, S.L., Xu, L., Li, L., et al., 2013. Sealing nuclear graphite with pyrolytic carbon. J. Nucl. Mater. 441 (1–3), 449–454.
Ferrari, A.C., 2007. Raman spectroscopy of graphene and graphite: disorder, electron–phonon coupling, doping and nonadiabatic effects. Solid State Commun. 143, 47–57.
Galy, N., Toulhoat, N., Moncoffre, N., Pipon, Y., Bérerd, N., Ammar, M.R., Simon, P., Deldicque, D., Sainsot, P., 2017. Ion irradiation to simulate neutron irradiation in model graphites: consequences for nuclear graphite. Instr. Meth. Phys. Res. B. 409, 235–240.
Gotoh, Y., Shimizu, H., Murakami, H., 1989. High resolution Electron microscopy of graphite defect structures after keV hydrogen ion bombardment. J. Nucl. Mater. 162–164, 851–**855**.
Irradiation Damage in Graphite Due to Fast Neutrons in Fission and Fusion Systems. IAEA Vienna 1011-4289.
Krishna, R., Wade, J., Jones, A.N., Lasithiotakis, M., Mummery, P.M., Marsden, B.J., 2017. An understanding of lattice strain, defects and disorderin nuclear graphite. Carbon 124, 314–333.
Kwiecinska, B., Suárez-Ruiz, I., Paluszkiewicz, C., Rodriques, S., 2010. Raman spectroscopy of selected carbonaceous samples. Int. J. Coal Geol. 84, 206–212.
Latham, C.D., Heggie, M.I., Alatalo, M., Öberg, S., Briddon, P.R., 2013. The contribution made by lattice vacancies to the Wigner effect in radiation-damaged graphite. J. Phys. Condens. Matter 25 135403.
Li, Z.Q., Lu, C.J., Xia, Z.P., Zhou, Y., Luo, Z., 2007. X-ray diffraction patterns of graphite and turbostratic carbon. Carbon 45, 1686–1695.
Li, M., Shi, C., Schut, H., Zhang, Z., Li, Z., 2019. The evolution of He+ irradiation-induced point defects and helium retention in nuclear graphite. J. Nucl. Sci. Technol. 56 (8), 744–751.
Maultzsch, J., Reich, S., Thomsen, C., 2004. Double-resonant Raman scattering in graphite: interference effects, selection rules, and phonon dispersion. Phys. Rev. B. 70, 155403.
Mironov, B.E., Freeman, H.M., Brown, A.P., Hage, F.S., Scott, A.J., Westwood, A.V.K., Da Costa, J.-P., Weisbecker, P., Brydson, R.M.D., 2015. Electron irradiation of nuclear graphite studied by transmission electron microscopyand electron energy loss spectroscopy. Carbon 83, 106–117.
Mitchel, E.W.J., Taylor, M.R., 1965. Mechanism of stored-energy release at 200° C in electron-irradiated graphite. Nature 208, 638–641.
Nemanich, R.J., Solin, S.A., 1979. First and second order Raman scattering from finite-size crystals of graphite. Phys. Rev. B. 20 (2), 392–401.
Ni, Z., Wang, Y., Yu, T., Shen, Z., 2010. Raman spectroscopy and imaging of graphene. Nano. Res. 1, 273–291.
Niwase, Keisuke, Tanabe, Tetsuo, 1993. Defect structure and amorphisation of Graphite irradiated by D^+ and He^+. Mater. Trans., JIM 34 (11), 1111–1121.
Pellemoine, F., Avilov, M., Bender, M., Ewing, R.C., Fernandes, S., Lang, M., Li, W.X., Mittig, W., Schein, M., Severin, D., Tomut, M., Trautmann, C., Zhang, F.X., 2015. Study on structural recovery of graphite irradiated with swift heavy ions at high temperature. Nucl. Instrum. Methods Phys. Res. B. 365, 522–524.
Production of atomic displacements by high-energy particles. Am. J. Phys. 24, 246.
Rosenthal, M.W., Haubenreich, P.N., Briggs, R.B., 1972. The Development Status of Molten–Salt Breeder Reactors. ORNL-4812.
Saha, U., et al., 2018. Neutron radiation damage studies in the structural materials of a 500 MWe fast breeder reactor using DPA cross-sections from ENDF/B-VII.1. Pramana - J. Phys. 90, 46.
Shi, C.Q., Schut, H., Li, Z.C., 2016. Thermal annealing of C ion irradiation defects in nuclear graphite studied by positron annihilation. J. Phys. Conf. Ser. 674 012019.
Sigmund, P., 2004. Stopping of Heavy Ions: A Theoretical Approach. Springer Verlag.
Spohr, R., 1990. Ion Tracks and Microtechnology. Vieweg Verlag.
Tan, Xing, Li, Lu Hua, Hou, Li ting, Hu, Xiaoping, Zhou, Shaoxiong, Peter, Robert, 2013. Mlade petravic, ying chen disorder in ball-milled graphite revealed by Raman spectroscopy. Carbon 57, 515–519.
Tang, Z., Hasegawa, M., Shimamura, T., Nagai, Y., Chiba, T., Kawazoe, Y., Takenaka, M., Kuramoto, E., Iwata, T., 1999. Phys. Rev. Lett. 82, 2532.
R. H. Telling and M. I. Heggie, Philos. Mag. 87, 4797.
Telling, R.H., Heggie, M.I., 2007. Radiation defects in graphite. Philos. Mag. 87 (31), 4797–4846.
Tian, L., Wen, M., Chen, J., 2010. Treatment and disposal of the radioactive graphite waste. In: Proceedings of the 18th International Conference on Nuclear Engineering, ICONE18-29985.
Zhang, Wen-ting, Zhang, Bao-liang, Song, Jin-liang, Qi, Wei, He, Xiu-jie, Liu, Zhan-jun, Lian, Peng-fei, He, Zhou-tong, Gao, Li-na, Xia, Hui-hao, Liu, Xiang-dong, Zhou, Xing-tai, Sun, Li-bin, 2016. Xin-xin Wu, Microstructure and molten salt impregnation characteristics of a micro-fine grain graphite for use in molten salt reactors. N. Carbon Mater. 31 (6), 585–593.
Zhou, Z., Bouwman, W.G., Schut, H., van Staveren, T.O., Heijna, M.C.R., Pappas, C., 2017. Influence of neutron irradiation on the microstructure of nuclear graphite: an X-ray diffraction study. J. Nucl. Mater. 487, 323–330.
Ziegler, J.F., Ziegler, M.D., Biersack, J.P., 2010. {SRIM} – the stopping and range of ions in matter. Nucl. Instrum. Methods Phys. Res. Sect. B Beam Interact. Mater. Atoms 268 (11–12), 1818–1823 2010.